Aeolian Research 31 (2018) 19–27

Contents lists available at ScienceDirect

Aeolian Research

journal homepage: www.elsevier.com/locate/aeolia

Measuring spatial and temporal variation in surface moisture on a coastal beach with a near-infrared terrestrial laser scanner

Yvonne Smit *, Gerben Ruessink, Laura B. Brakenhoff, Jasper J.A. Donker

Department of Physical Geography, Faculty of Geosciences, Utrecht University, PO Box 80.115, 3508 TC, Utrecht, The Netherlands

ARTICLE INFO

Article history:
Received 9 May 2017
Revised 30 June 2017
Accepted 10 July 2017
Available online 22 July 2017

Keywords:
Terrestrial laser scanner
Near-infrared
Surface moisture
Coastal
Calibration curve
Aeolian sand transport

ABSTRACT

Wind-alone predictions of aeolian sand deposition on the most seaward coastal dune ridge often exceed measured deposition substantially. Surface moisture is a major factor limiting aeolian transport on sandy beaches, but existing measurement techniques cannot adequately characterize the spatial and temporal distribution of surface moisture content. Here, we present a new method for detecting surface moisture at high temporal and spatial resolution using a near-infrared terrestrial laser scanner (TLS), the RIEGL VZ-400. Because this TLS operates at a wavelength (1550 nm) near a water absorption band, TLS reflectance is an accurate parameter to measure surface moisture over its full range. Five days of intensive laser scanning were performed on a Dutch beach to illustrate the applicability of the TLS. Gravimetric surface moisture samples were used to calibrate the relation between reflectance and surface moisture. Results reveal a robust negative relation for the full range of possible surface moisture contents (0%–25%), with a correlation-coefficient squared of 0.85 and a root-mean-square error of 2.7%. This relation holds between 20 and 60 m from the TLS. Within this distance the TLS typically produces O(10^6–10^7) data points, which we averaged into surface moisture maps with a 1 × 1 m resolution. This grid size largely removes small reflectance disturbances induced by, for example, footprints or tire tracks, while retaining larger scale moisture trends.

1. Introduction

The most seaward coastal dune ridge is often highly dynamic because of the alternation between intense marine erosion during severe storms and more gentle aeolian deposition during prolonged (seasons – years) fair-weather conditions. Where models to predict marine dune erosion exist (Roelvink et al., 2009) and can be used in operational and scientific settings, similar quantitative models for aeolian transport and dune growth are only just appearing (Delgado-Fernandez, 2011; Keijsers et al., 2016). Simple aeolian transport models that rely on wind characteristics alone, generally overpredict measured dune growth considerably, pointing to beach characterstics as a limiting source for aeolian transport (Keijsers et al., 2016; Delgado-Fernandez, 2011; Davidson-Arnott and Law, 1996).

Surface moisture is believed to be a major limiting factor to aeolian sand transport (Davidson-Arnott et al., 2005; Wiggs et al., 2004; Atherton et al., 2001; McKenna Neuman and Scott, 1998; Sarre, 1988). It is a primary control on the development of the fetch effect on beaches and increases the shear velocity threshold required to entrain sediment (Delgado-Fernandez, 2010; Bauer and Davidson-Arnott, 2002). Therefore it is of interest to accurately account for surface moisture in aeolian transport modelling (Hesp et al., 2009; Delgado-Fernandez and Davidson-Arnott, 2009; Walker et al., 2009; Bauer and Davidson-Arnott, 2002; Fecan et al., 1999; McTainsh et al., 1998; Marticorena and Bergametti, 1995). However, conventional measurement techniques cannot adequately characterize the distribution of surface pore water content over a continuous horizontal plane (Darke and McKenna Neuman, 2008). While measurement techniques such as soil moisture probes can be very useful at elucidating spatial moisture patterns in the intertidal zone and back beach area (Schmutz and Namikas, 2011; Namikas et al., 2010; Anthony et al., 2009), they measure moisture content averaged over a layer of sand, rather than the actual surface which is most important for aeolian sand transport (Nield et al., 2011; Darke et al., 2009). The traditional gravimetric method, which involves removing a known volume of soil sample from the field and determining the mass of water content in relation to the mass of the dry soil, is accurate but also has a number of disadvantages. For example, obtaining a uniform thickness of sampling and a repeated measurement at the exact same location is impossible due to the destructive nature of the methodology, which limits its use to quantify temporal and spatial

* Corresponding author.
E-mail address: y.smit@uu.nl (Y. Smit).

http://dx.doi.org/10.1016/j.aeolia.2017.07.004
1875-9637/

variability in surface moisture (Tsegaye et al., 2004; Hillel, 1980). The optical brightness method (Darke et al., 2009) is, on the other hand, non-destructive and continuously tracks pore water variability at the beach surface through time and space (during daylight hours), but it requires careful control for changing illumination, as well as regular calibration against gravimetric measurements (Darke et al., 2009; Darke and McKenna Neuman, 2008). Instead of using destructive and time-consuming methods, terrestrial laser scanning may be a faster and repeatable remote sensing method that evaluates the top of the surface and gives a more representative measure of the spatial and temporal variation of surface moisture (Nield et al., 2011; Kaasalainen et al., 2010).

Nield et al. (2014) used a time-of-flight Leica Scanstation that utilizes a green laser (wavelength $\lambda = 532$ nm) to illustrate that the return signal intensity is related to surface moisture. To be more specific, Nield et al. (2014) found that at distances less than 20 m the return signal intensity increased with distance, whilst for distances over 20 m from the sensor the return signal intensity decreased with distance. Additionally, Nield et al. (2014) showed that the intensity values can discriminate within 1–2% gravimetric moisture content over the lower gravimetric moisture content range between 0% and 6%. However, the corresponding TLS intensities varied in a very narrow range. Hence, they suggested that a TLS utilizing more moisture sensitive (e.g., infrared; Edwards et al., 2013; Nolet et al., 2014) or multispectral wavelengths may be able to detect surface moisture over a larger range and with higher precision.

In this paper we examine the suitability of a shortwave near-infrared TLS (RIEGL VZ-400, wavelength $\lambda = 1550$ nm) to measure the spatial and temporal variation in surface moisture content on a coastal beach. Based on several deployments on Egmond beach, the Netherlands, we examine the robustness of the measurements, quantify the distance over which the measurements are reliable as a surface moisture proxy, and derive a calibration curve based on gravimetric moisture samples. As the TLS spatially oversamples moisture content, we also explore how averaging the data into regular grids with different resolutions affects noise levels, while at the same time resolves true spatial variability. We start with a brief theoretical description of why the returned signal contains surface moisture information. This description guides the processing of our TLS data.

2. Theory

A terrestrial laser scanner (TLS) is an active remote sensing technique that utilizes the round trip time of an emitted laser beam to provide the range between the laser scanner and the backscattering object (Wagner et al., 2006). A TLS derives useful object representations by means of a dense three-dimensional (3D) point cloud and is therefore used routinely for topographic mapping, forest measurements or 3D city models (Heritage, 2009; Höfle and Pfeifer, 2007). To measure surface moisture the important variable is the returned intensity of the emitted beam (I_R), which depends on the backscattering characteristics of the target, measurement geometry and various sensor parameters. The fundamental relation to explain I_R is the radar equation (Wagner et al., 2006),

$$I_R = \frac{I_T D_r^2}{4\pi R^4 \beta_t^2}\sigma. \quad (1)$$

Here, I_T is the transmitted power, D_r is the aperture of the receiver optics, R is the range (distance to target), β_t is the transmitted beam width and σ is the so-called backscatter cross-section which reads

$$\sigma = \frac{4\pi}{\Omega}\rho A_s. \quad (2)$$

Here Ω characterizes the directionality of scattering, which is different for smooth and rough surfaces, ρ represents the reflectivity of the target, and A_s is the receiving area of the scatterer (Wagner et al., 2006). If we assume this area to be circular, A_s can be written as

$$A_s = \frac{\pi\beta^2 R^2}{4}. \quad (3)$$

The substitution of Eqs. (2) and (3) into Eq. (1), and the assumption that I_T, D_r and Ω are constant during a laser survey (Kaasalainen et al., 2011), implies that I_R is a function of ρ and R as

$$I_R = f\left(\frac{\rho}{R^2}\right). \quad (4)$$

As R is known for each target, the decay of I_R with R^2 can be corrected to result in

$$T = f(\rho), \quad (5)$$

where we call T the reflectance. The reflectivity of beach sand depends predominantly on its surface moisture content. This dependence is negative, hence a lower ρ indicates a higher moisture content (Nolet et al., 2014; Edwards et al., 2013; Kaasalainen et al., 2010; Lobell and Asner, 2002). To summarize, in this paper we examine the relationship between range-square corrected return intensity (i.e., reflectance T) and moisture content.

3. Deployment

3.1. Study site

Measurements with a RIEGL VZ-400 TLS were performed at the beach of Egmond aan Zee, The Netherlands. Egmond aan Zee is located on the approximately 120 km long, roughly north–south oriented central Holland coast (Fig. 1). This micro- to meso-tidal site is wave-dominated and has a relatively narrow (~100 m maximum at spring low tide), mildly sloping (~1:30) beach consisting predominantly of quartz sand with a median diameter of about 250 μm. The intertidal zone usually contains a single slip-face bar. The foredune at Egmond aan Zee is ~25 m high with a steep seaward facing slope because of occasional erosional events in winter (e.g., De Winter et al., 2015) and is largely covered by European marram grass (*Ammophila arenaria*).

The RIEGL VZ-400 was deployed five times, on December 6, 2012, April 29, 2013, March 27, 2015, September 29, 2015 and October 29, 2015. On all days the TLS was positioned some 10 m landward of the high-tide line in view of one of the cameras of the Egmond Coast3D Argus tower (Van Enckevort and Ruessink, 2001; Fig. 1). This has the benefit of having a detailed visual account on where the TLS was positioned relative to the beach morphology and the (time-shifting) waterline. On April 29, 2013 the TLS was positioned north of the Argus Tower, near local beach pole 40.50, while on all other days the TLS was located somewhat further south, near local beach pole 41.50.

3.2. RIEGL VZ-400 TLS

The RIEGL VZ-400 operates in the shortwave near-infrared at $\lambda = 1550$ nm, hence close to the water absorption peak of 1470 nm (e.g., Lobell and Asner, 2002; Wallace and Hobbs, 2006; Nolet et al., 2014). The RIEGL VZ-400 has an effective measurement rate of 122,000 points/s and a beam divergence of 0.30 mrad. Each

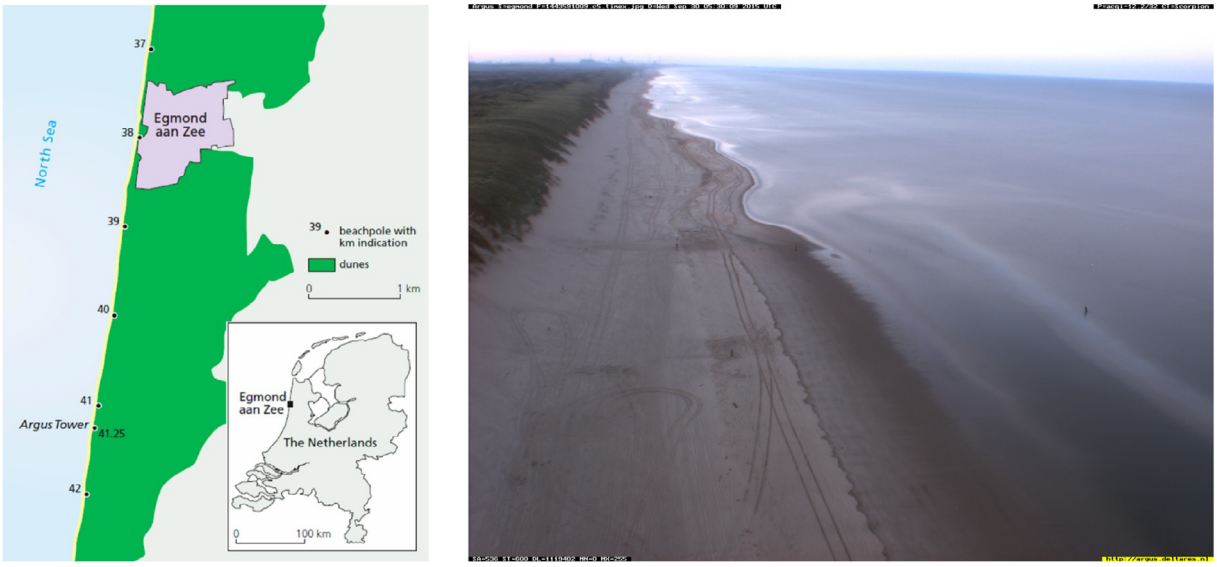

Fig. 1. (left) The study site Egmond aan Zee in The Netherlands (right) picture of Egmond beach, between beach poles 41 and 42, taken in the southern direction by an Argus video camera.

point is associated with a horizontal angle ϕ and a vertical angle θ. Here, the TLS was set up to have $\phi = 0°$ in the cross-shore direction towards the dune; $\theta = 0°$ is vertically upward. Each (ϕ, θ, R) coordinate is automatically converted into Cartesian (x, y, z) coordinates, which are relative to the TLS. During each deployment four retro-reflective cylinders were placed in an approximate rectangle around the TLS. Their positions were obtained with an RTK-GPS and were used to convert the scanner's (x, y, z) into a local coordinate scheme, where x and y are cross-shore and alongshore coordinates, respectively, and z is elevation with respect to Mean Sea Level (MSL). Each point also has a value of I_R.

3.3. Line scans & panoramic scans

The TLS can be operated in two different ways resulting in a line or panoramic scan, respectively. In a line scan ϕ is fixed (i.e. no horizontal rotation; we used $\phi = 0°$ and $\phi = 180°$), while θ goes repeatedly from its minimum (80°) to its maximum (130°). In this way $z(x)$ and $I_R(x)$ are obtained for a fixed y. With the applied θ step of 0.008°, approximately 600 profiles were scanned per minute. As a line scan was ceased after 2 min, it is safe to assume that surface moisture did not change during the scan. In other words, line scans are ideal to test the robustness (or repeatability) of the measurements.

In a panoramic scan ϕ changes from 0° to 360°, while for each ϕ, θ changes from 80° to 130°. In the present work the ϕ step size was 0.020° and the θ step size was 0.020°, resulting in a typical scan duration of 12 min. On December 6, 2012, April 29, 2013 and March 27, 2015 the measurement set-up was to first perform a panoramic scan and then the $\phi = 0°$ and $\phi = 180°$ line scans. This was repeated every 30 min. On September 29, 2015 and October 29, 2015 the line scans were omitted and a panoramic scan was carried out every 15 min.

Fig. 2 shows a typical output of a panoramic scan. Fig. 2a illustrates the bed elevation z, with the foredune ($z > 3$ m) on the right. Note the intertidal bar-trough morphology at $x \sim 475$ m. Fig. 2b shows the so-called amplitude, which is proportional to I_R, and defined as the ratio of the actual detected optical amplitude of the echo pulse to a detection threshold. The ratio is stated in decibels (dB). The amplitude is not corrected for range and thus shows concentric circles in a panoramic scan. Internally, the RIEGL VZ-400 recomputes amplitude with a $1/R^2$ correction into reflectance T. In more detail, T is defined as 10 times the base-10 logarithm of the ratio of I_R to the intensity I_0 of a diffuse flat white target at the same range as the target and with its surface normal pointing towards the laser scanner. A factor of 50% reflectance thus results in $T = -3$ dB and 1% gives $T = -20$ dB. Reflectance values above 0 dB indicate that the target gives an optical echo amplitude larger than that of a diffuse white target, i.e., the target is (partially) retro-reflecting. As can be seen in Fig. 2c, the $1/R^2$ correction inherent to the computation of T removes the concentric circles and the T values now follow the morphology (compare to Fig. 2a). The largest T is found on the upper beach (~ -4 to -8 dB), where one would expect the lowest moisture content and decreases towards ~ -20 dB near the water line, with a slight increase on the sandbar. The lowest T is found in the trough, where the moisture content is presumably highest. Low values of T are also found higher up on the foredune, but these relate to marram grass rather than to wet sand.

Finally, Fig. 2d illustrates a non-dimensional measure called deviation that represents the difference between the form of the emitted and returned laser pulse. High deviations are found high on the foredune, and at distances in excess of some 50 m from the TLS in the alongshore direction. The former are presumably induced by multiple reflections from marram grass, while the latter are presumably caused by the increasingly non-circular footprint of the laser beams on the beach. These large deviations might indicate that T values at these large distances are less reliable than closer to the TLS.

3.4. Gravimetric surface moisture measurements

To relate T to surface moisture (w) the panoramic scans on March 27, September 29 and October 29, 2015 were used. A total of 10 panoramic scans per day were taken and after each panoramic scan, 10 surface moisture samples were collected in the area surveyed by the TLS. The surface moisture samples were taken from the upper centimeter with a spatula and collected in a sealable plastic bag. On March 27 two persons collected 10 samples over a cross-shore transect after each panoramic scan. However, collecting 10 surface moisture samples was rather time consuming. Accordingly, moisture content in the later samples may no longer relate to T because of temporal variability in moisture content. Therefore, on September 29 and October 29, 2015 four

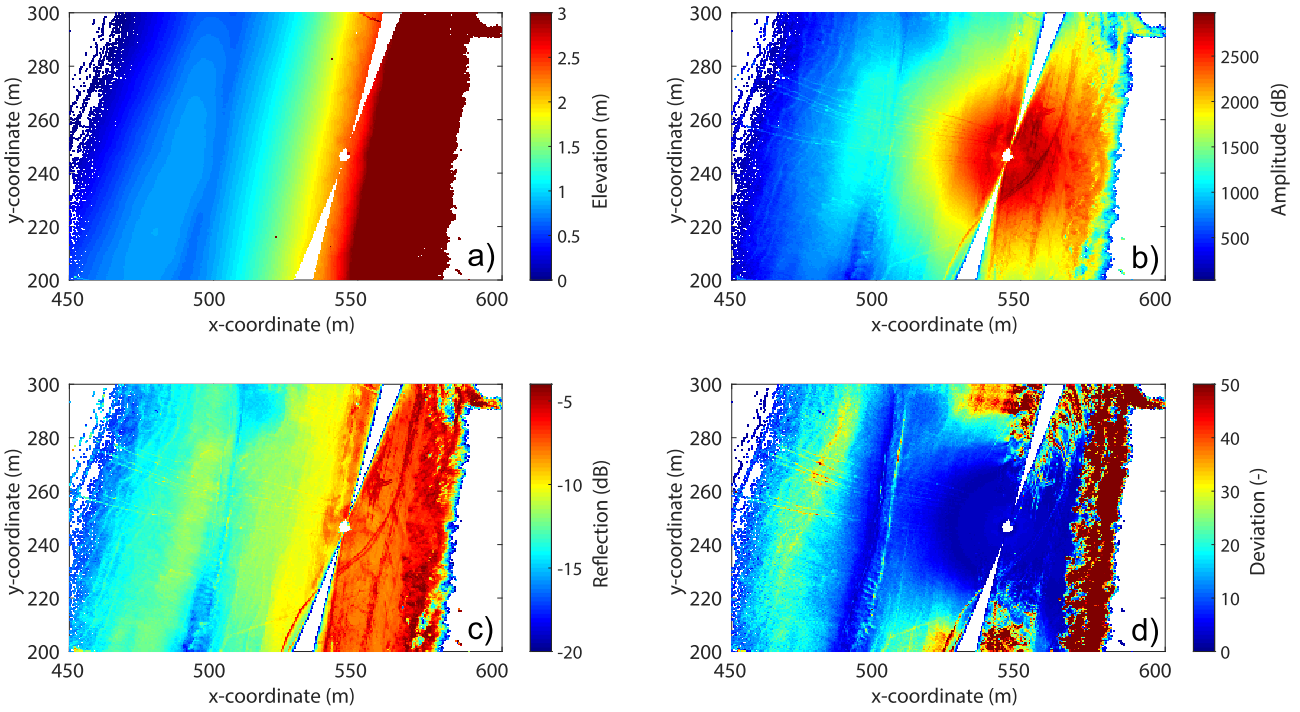

Fig. 2. Example of the main output variables of a panoramic scan made on March 27, 2015: (a) elevation z, (b) amplitude I_r, (c) reflection T and (d) deviation.

persons (two pairs) collected 5 surface moisture samples over a cross-shore transect after a panoramic scan. To be able to find the corresponding location in the panoramic scan, each location where surface moisture samples were taken was measured with an RTK-GPS and converted to the same local coordinate scheme used for the TLS. The analysis of the surface moisture content was done with the gravimetric method (Davidson-Arnott, 2010). In the laboratory the soil samples were weighted when wet and again after drying the samples in an oven on 105° C for 24 h.

4. Results

4.1. Robustness

To test the robustness of the TLS reflection measurements, the line scans were analyzed. Each set of line scans (~1200 per 2 min) was analyzed by calculating the mean and standard deviation for z and T at each θ. During the analysis errors in the reflectance data caused by waves in the swash zone and incidental off-terrain objects were noticed. To remove erroneous data, a θ threshold was imposed to guarantee that all data points reflected by waves in the swash zone were removed. This threshold angle differed for consecutive line scans, given the tide-imposed time-varying location of the swash zone. Additionally, points with a z more than 6 times the standard deviation in z were considered outliers (for example, humans walking or birds flying through the line scan) and hence removed from the data.

Fig. 3 shows the results for a representative line scan in the seaward (+55 m, swash zone) and landward (−40 m, dune foot) direction. The TLS is situated at 0 m. The mean z profile (Fig. 3a) slopes seaward, with a very subtle 'platform' sandbar at about 20 to 30 m seaward from the laser. Towards the dunes beach elevation increases and rises towards 8 m height where the line scan was truncated. Above 8 m height marram grass is located which moves with the wind and causes high standard deviations in the z profile and T values that are not representative for assessing the robustness. The standard deviation in z (s_z) is always less than 0.006 m (Fig. 3b), and mostly below 0.002 m. In more detail, s_z slightly increases with distance, especially in the seaward direction.

Fig. 3c shows the reflectance measurements. The black lines show all scan lines made in 2 min, wherein it is clearly visible that at a same distance reflectance can vary with 4 dB between individual line scans. From the dune foot towards the swash zone reflectance changes for the selected line scan from high (−6 dB) towards low values (−16 dB), presumably reflecting the change from dry to saturated sand. The black line in Fig. 3d shows the corresponding standard deviation of reflectance. Within 2 min surface moisture content did not change, hence the standard deviation shown in Fig. 3d with a maximum of 0.8 dB is caused by instrument noise. The standard deviation increases slightly with distance.

Because the TLS oversamples expected spatial variations in surface moisture (e.g. Fig. 3c), it is appropriate to average T observations in each individual scan line in bins with a certain cross-shore size as to reduce instrument noise. For each bin a new standard deviation can be computed. Fig. 4 illustrates the cross-shore average standard deviation as a function of bin size. As can be seen, this spatially averaged standard deviations decreases with bin size to ~ 0.07 dB at a bin size of 1 m. We consider this bin size still to be sufficiently fine to capture spatial moisture variability.

The red lines in Fig. 3c and d are the reflectance and its standard deviation, respectively, using a bin size of 1 m. The number of data points in the bin is provided in Fig. 3e. As can be seen in Fig. 3d, the standard deviation is now mostly below 0.2 dB, with an increase to ~0.6 dB near the swash zone, where the number of data points is lowest (Fig. 3e). Even a value of 0.6 dB is rather low ($\sim< 6\%$). Near the swash zone the number of data points (~10 per m) is still substantially higher than generally achievable with, for example, a Delta-T theta probe or with surface samples. On the whole, Fig. 3d illustrates that, after modest spatial averaging, reflectance T is a highly repeatable (i.e. robust) measure.

4.2. Range

To investigate the influence of the range on reflectance we explored an alongshore transect in the panoramic scans taken on

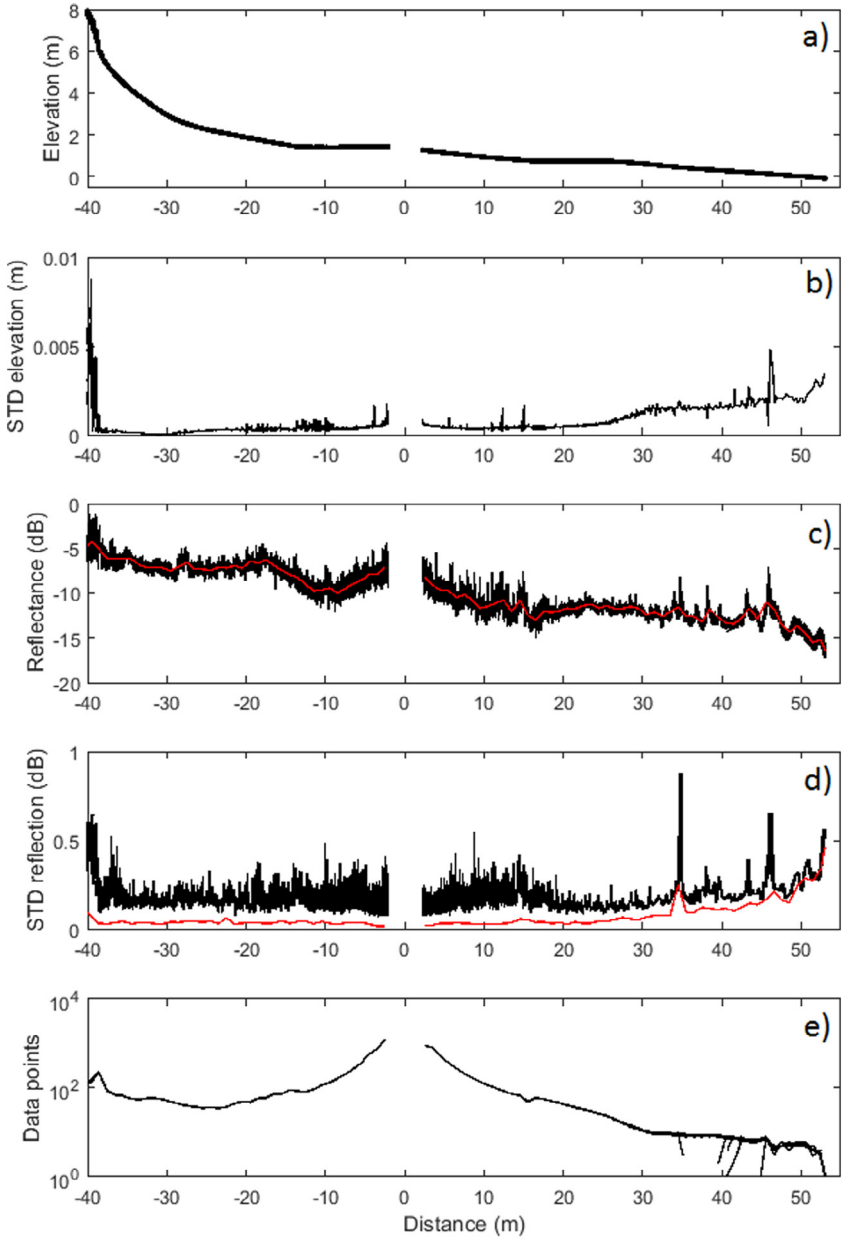

Fig. 3. Line scan characterstics, made on April 29, 2013 at 14:49:36 during low tide. Each graph shows the position of the TLS at 0 m, the upper beach towards −40 m where marram grass is located and the intertidal beach until 55 meters where the swash zone starts. (a) Shows the beach elevation (m) relative to mean sea level. (b) Is the standard deviation of the beach elevation calculated with 1200 line scans. (c) Shows the reflectance measurements of all 1200 line scans in black and the mean in red, of which all data points are averaged over 1 m. (d) Shows the standard deviation of reflectance in black, made with a total of 1200 line scans and the red line represents the standard deviation after averaging the datapoints over a grid resolution of 0.25 m. (e) Shows the amount of data points per gridbox over distance. (For interpretation of the references to colour in this figure caption, the reader is referred to the web version of this article.)

December 6, 2012 and April 29, 2013 when the beach morphology was relatively flat and alongshore uniform. We can assume that, in the alongshore direction variations in moisture were small, resulting in approximatley alongshore constant reflectance. To minimize instrument noise, yet to retain any true reflectance trends, the 3D point clouds were processed into 1×1 m bins. Fig. 5 shows a represenative alongshore from December 6, 2012, where zero is the position of the TLS and −100 m is the northward direction and +100 m the southward direction. Within the first $\sim$20 m T decreases markedly. This was found in most other scans too, and presumably reflects that the $1/R^2$ correction is not appropriate so close to the TLS. Similar TLS-induced reflectance behaviour was also noted by Nield et al. (2014) for another TLS. Beyond 20 m T stays approximately constant up to about 60 m, where T drops off and the data becomes gappy. These data gaps are caused by a reduced density of the point cloud due to a small angle of incidence and the large range. From Fig. 2d we already noted that at these large distances the emitted and returned pulse differ and that reflectance may no longer be accurate. Based on Fig. 5 and other panorama scans of the two selected days, we presume reflectance measurements to be accurate when the range is between 20 and 60 m. This distance of 60 m corresponds to an angle of incidence

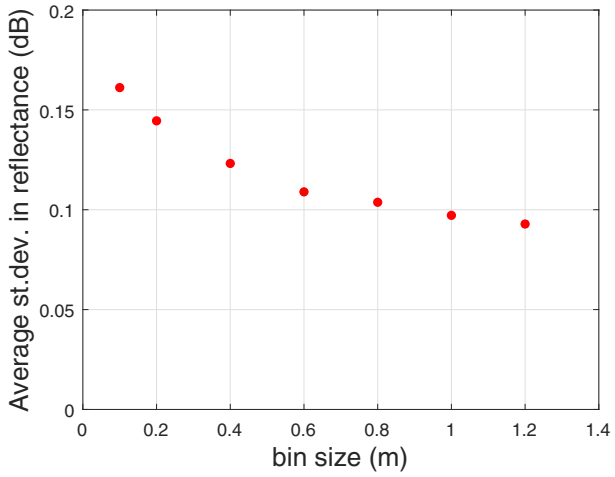

Fig. 4. Spatially averaged standard deviation of reflectance of a line scan versus grid size.

of 88° (i.e., angle between beach surface normal and laser beam), given that the TLS height was 1.83 m above beach level in this situation. We return to this value in Section 5.

4.3. Calibration curve

To quantify the relationship between surface moisture and reflectance the locations of the surface moisture samples were connected to a corresponding 1 × 1 m grid cell in the panoramic scan. The corresponding median reflectance (dB) in the grid cell was compared with the gravimetric surface moisture content to produce a calibration curve. We chose the median rather than the mean because many panoramic scans showed small-scale variations in reflectance, see Figs. 3 and 6, and Section 5.2. As the 1 × 1 m size is larger than these disturbances, they do not affect the median. For grid cells without disturbances, the median and mean are essentially identical. In addition, all surface moisture samples that were taken close to a footprint, tire track or within the swash zone were not considered further.

Fig. 7 illustrates that reflectance T was related to surface moisture over its full range from dry ($\sim 0\%$) to saturated (20–25%) sand. Given the observed dependence, the following sigmoidal curve was fit

$$\widetilde{w}(T) = \frac{w_{min} - w_{max}}{1 + e^{-a(T-c)}} + w_{max}, \tag{6}$$

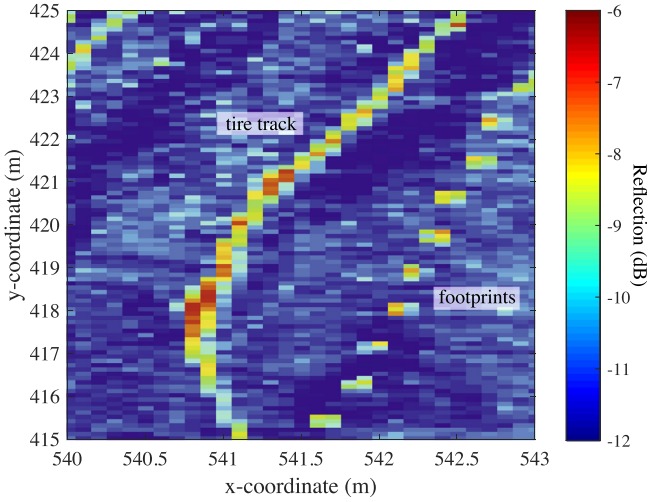

Fig. 6. Example of non-moisture induced reflectance, here tire tracks and footprints.

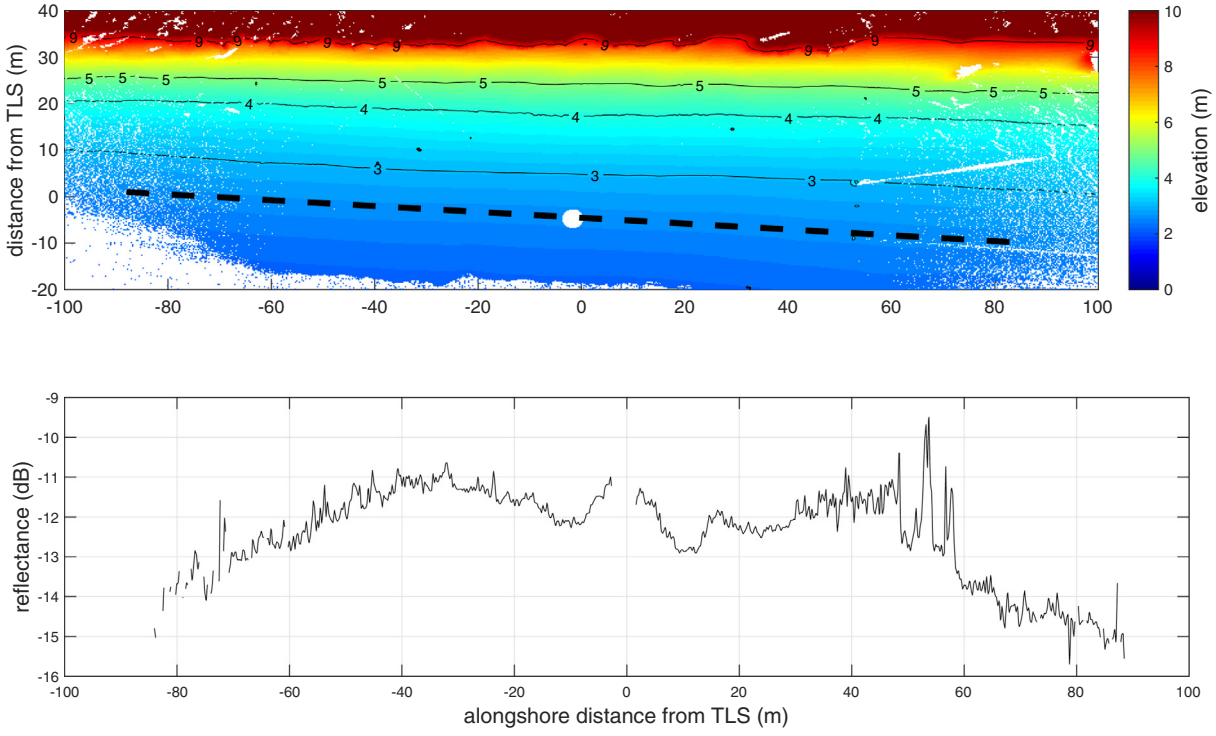

Fig. 5. Range of reflectance over an alongshore transect extracted from a panoramic scan made December 6, 2012 at 14:24:01 when the topography was almost flat and surface moisture varied minimal. On the *x*-axis the distance is plotted where at 0 m the TLS is situated. On the *y*-axes reflectance is plotted varying from −11 dB to −15 dB. Note the drop in reflectance within the first 20 m and the data gaps in reflectance after 60 m.

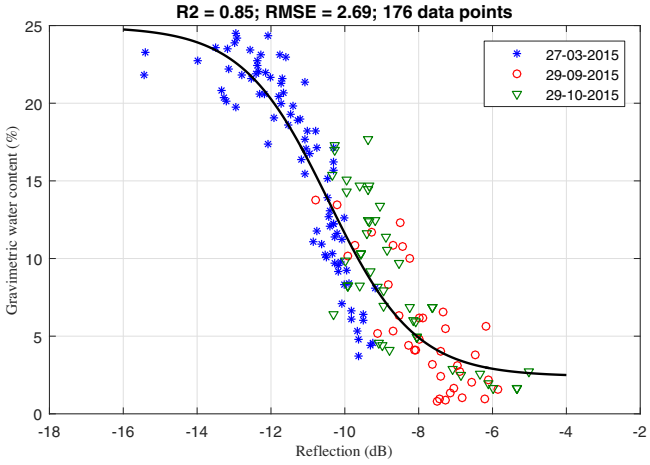

Fig. 7. Calibration curve fitted with a sigmoid fit, made with 176 data points measured over 3 days of TLS surveys.

where $\widetilde{w}$ is a predicted moisture value, and a and c are fit parameters. Here a determines the slope of the sigmoidal fit, c is the centre of the dataset, and w_{max} and w_{min} represent the asymptotes, hence saturation and dry soil, respectively. A least squares fit yielded $a = 0.86 \pm 0.24$ and $c = -10.43 \pm 0.31$ dB where $\pm$ indicates the 95% confidence band. The correlation-coefficient squared (R^2) has a value of 0.85 and the root-mean-square error (RMSE) is 2.69%.

4.4. Application

Three 1×1 m surface moisture maps taken on September 29, 2015 over falling tide are shown in Fig. 8 as an example application of the calibration curve. The maps give a clear illustration of how surface moisture fluctuates over space and time with corresponding beach elevation (Fig. 8d). The lighter yellow colors indicate a low surface moisture content, which are visible on the back beach in front of the dunes. Surface moisture contents at the back beach above the high water line (the 1-m contour) vary spatially from 0% until 8% surface moisture content. Toward the sea, surface moisture increases, depicted with green, blue to dark blue colors. Surface moisture in the intertidal zone varies spatially from 10% surface moisture towards complete saturation of 25%. No data points are visible in the trough. This can be ascribed to the fact that the trough is inundated by water, which absorbs the laser beam. In contrast, the sandbar shows lower moisture contents than its surroundings. Some unnatural features are visible like tire tracks, which appear drier than their surroundings as well (see Fig. 6).

Over time the intertidal zone dries out towards the sea and the sandbar also shows clear evidence of dessication. The trough dries out as well, as more data points become visible in the trough over time, which means that the trough is not fully inundated anymore. Over five hours the intertidal beach dries out with a value varying between 6% and 14.5% surface moisture. Furthermore, dry out rates up to 8% surface moisture per hour are observed. In future work we will analyze all obtained moisture maps to more fully quantify the

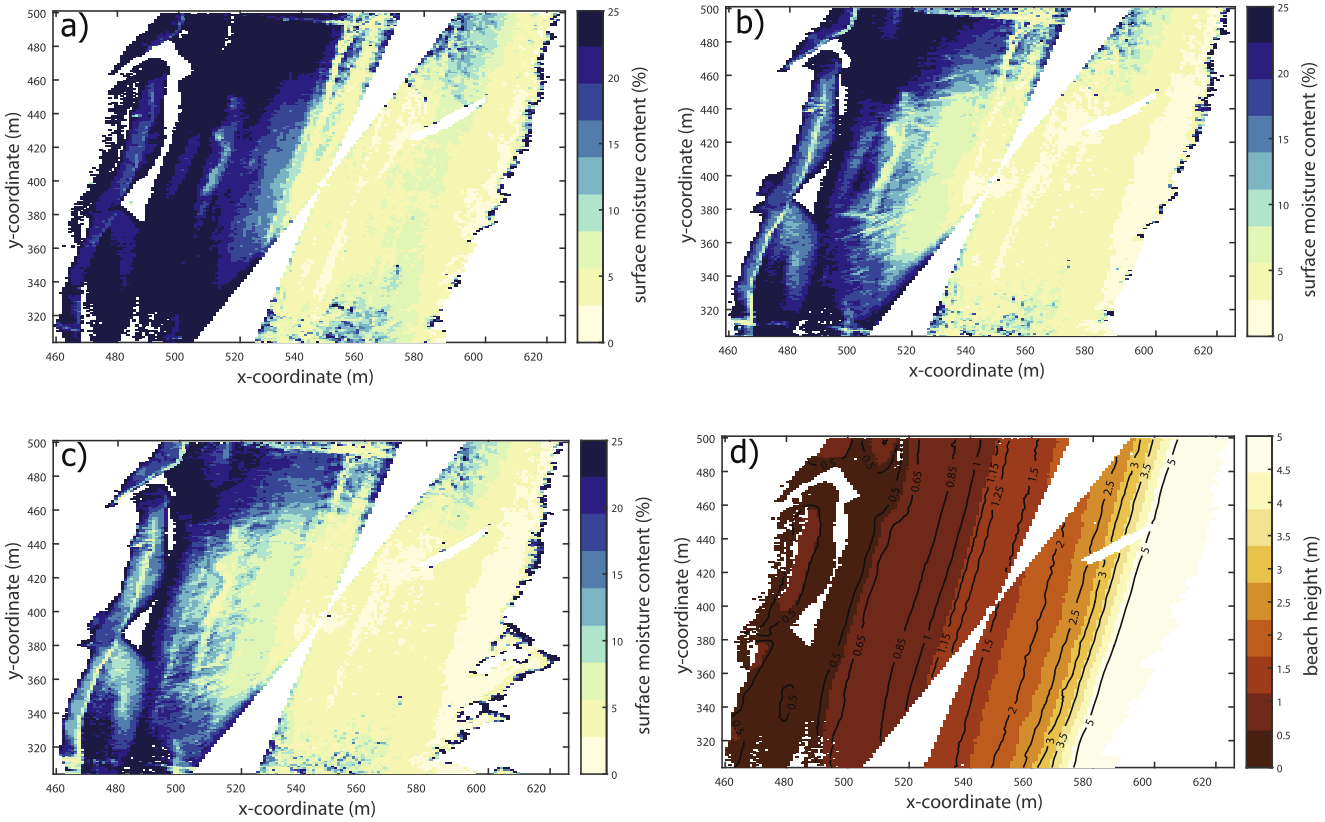

Fig. 8. Three surface moisture maps that show the surface moisture variations during falling tide on September 29, 2016 at the beach of Egmond aan Zee, with a corresponding beach height. On the right side the dunes are situated and on the left side the sea. A clear trough at approximately 480 m in the x-coordinate is visible, which dries out during the day. Also the yellow colour spreads out towards the sea, which means the soil dries up during the day. Graph (a) was taken at 10:30 h, (b) at 14:00 h, (c) at 16:00 h. (d) Shows the beach height above mean sea level on September 29, 2016. (For interpretation of the references to colour in this figure caption, the reader is referred to the web version of this article.)

spatial and temporal surface-moisture variability and to determine its underlying causes.

5. Discussion

We have shown that the reflectance output of the near-infrared RIEGL-VZ 400 is a robust and accurate parameter to measure surface moisture over its range of 0% to 25%. This is an improvement over the earlier TLS results of Nield et al. (2014), who covered the 0 to 6% range only with a green laser. In our case a sigmoidal curve describes the relationship between reflectance and surface moisture with a RMSE of 2.7%. In comparison to (modified) theta probes with a RMSE of $\pm 2\%$ (Schmutz and Namikas, 2011) and the optical brightness method with a RMSE on the order of 3–4% (Darke et al., 2009), a near-infrared TLS is an accurate technique to measure surface moisture from the thin upper layer. In its present set-up the calibration curve is applicable for distances of ~20 m to 60 m from the TLS. A serious drawback of using a TLS to measure surface moisture is its high purchase costs relative to theta probes or even an optical system. This may prevent widespread TLS use to quantify spatial and temporal moisture patterns on a coastal beach. In addition, the amount of surface moisture samples we used to produce the calibration curve substantially exceeds those used in calibrating theta probes (~ 30; Atherton et al., 2001; Tsegaye et al., 2004). Therefore, we tested if this amount could be reduced by taking N (N ranging from 10 to 175) samples from our sampling pool and determining the RMSE. We repeated this 1000 times and determined the maximum RMSE for each N over those 1000 tries. The RMSE does not exceed 3% for $N > 85$. This means that half the amount of soil samples we took over the full range of surface moisture content should be sufficient to determine the calibration curve. We now discuss the effects of angle of incidence of the laser beam, surface roughness, and grain size and mineralogy on our observed dependence of reflectance on moisture content.

5.1. Angle of incidence

The angle of incidence influences the maximum distance over which a TLS can accurately measure surface moisture. It is highly dependent on target physical properties and geometrical conditions (Pesci and Teza, 2008). In our case the physical properties are controlled by the grain size of the beach sand with a D50 of ~250 micrometers and the geometrical conditions are controlled by the height of the TLS, which was kept at about 1.8 m, and surface roughness, which on the beach is very low. These properties resulted in accurate reflectance measurements until a distance of 60 m with a corresponding angle of incidence of 88°. Beyond 60 meters the assumption of a circular laser footprint is apparently so violated that the R^2 correction breaks down. This is also reflected from the marked increase in deviation (Fig. 2d) beyond 60 m from the TLS.

It is perhaps surprising that T does not depend on θ for θ up to 88°. Many environmental surfaces have Lambertian scattering properties, in which case the backscatter cross-section σ, and hence I_R and T, have a $cos(\theta)$ proportionality (Jensen, 2007). Apparently, sand grains act as macroscopic irregularities within a laser footprint; in other words, there are always -even at large θ- sufficient parts of the grains that are perpendicular to the incident beam to neutralize the Lambertian cosine law. Our finding that sand acts non-Lambertian is consistent with TLS experiments with sand-like material laboratory set-up, in which I_R was also found to be largely independent of θ, even for θ above 60° (Pesci and Teza, 2008; Kukko et al., 2008; Kaasalainen et al., 2011).

5.2. Surface roughness

TLS reflectance is sensitive to changes in roughness of the reflecting surface (Pesci and Teza, 2008; Kukko et al., 2008). In our case tire tracks and footprints are clearly visible as roughness elements on an otherwise flat beach and show a higher reflectance than the immediate surroundings. Apparently, roughness (Ω) in the radar equation cannot always be assumed to be constant. By using a 1×1 m gridsize and the median rather than mean reflectance, such disturbances can largely be removed, while retaining larger scale trends. It has to be noted that tire tracks also cause sand to dry out faster, as observed during our measurement days (see Fig. 6). Thus, the higher reflectance output of tire tracks may not entirely be ascribed to roughness only.

5.3. Grain size & mineralogy

Other parameters that can influence the reflectance besides surface moisture and roughness, are grain size and mineralogy of the sand. However, the mineralogy and grain size distribution during a fieldwork campaign are unlikely to change hugely. Therefore, when using the TLS one day of calibration is needed and from there it can be used for the entire campaign on the same location. Furthermore, Leu (1977) indeed found a relationship between grain size (D50 varying from 320 to 950 μm) and reflectance but only for the visible part of the wavelength. Also, in his data there is no clear relationship between mineralogy reflectance beyond a wavelength of 1.38 μm. As wavelength increases the influence of moisture is dominant over mineralogy and grain size (Watson, 1970; Leu, 1977; Shuchman and Rea, 1981). Hence, our calibration curve for the RIEGL-VZ 400 to measure surface moisture can be used for most sandy beaches with a D50 around 250 μm. However, one day of calibrating reflection output to surface moisture is recommended nonetheless.

6. Conclusion

We have shown that the reflectance output of the near-infrared RIEGL-VZ 400 is a robust parameter to measure surface moisture from the thin upper layer over its full range from 0% to 25%. This thus includes the range of surface moisture content between 0% and 8% where the threshold lies for aeolian transport. The calibration curve of the presented TLS, describing the relationship between reflectance and surface moisture, has a correlation coefficient squared of 0.85 and a root-mean-square error of 2.7%. The latter is comparable to the often used Delta-T theta probe. The curve is applicable for distances of 20 m to 60 m from the TLS, although this distance likely depends on the height of the TLS above the beach. Parameters like surface roughness, grain size and mineralogy also influence the relationship between reflectance and moisture content but the effect of surface moisture dominates. As long as one day of calibrating surface moisture to reflectance is performed per fieldwork campaign, TLS (RIEGL-VZ 400) is an highly suited technique to accurately and robustly measure spatiotemporal surface moisture variations on a coastal beach with high spatial (~ 1×1 m) and temporal (~ 15—30 min.) resolution.

Acknowlegdgements

This research is supported by the Dutch Technology Foundation STW, which is part of the Netherlands Organisation for Scientific Research (NWO), and which is partly funded by the Ministry of Economic Affairs (contract 13709). Marcel van Maarseveen, Henk Markies, Chris Roosendaal, Arjan van Eijk, Winnie de Winter, Pam Hage, Jantien Rutten, Lianne van der Weerd, Bram Slinger

and Cees Smit -in particular- are greatly thanked for their help and support during the TLS surveys.

References

Anthony, E.J., Ruz, M., Vanhee, S., 2009. Aeolian sand transport over complex intertidal bar-trough beach topography. Geomorphology 105, 95–105.

Atherton, R.J., Baird, A.J., Wiggs, G.F.S., 2001. Inter-tidal dynamics of surface moisture content on a meso-tidal beach. J. Coastal Res. 17 (2), 482–489.

Bauer, B.O., Davidson-Arnott, R.G.D., 2002. A general framework for modeling sediment supply to coastal dunes including wind angle, beach geometry, and fetch effects. Geomorphology 49, 89–108.

Darke, I., McKenna Neuman, C., 2008. Field study of beach water content as a guide to wind erosion potential. J. Coastal Res. 245, 1200–1208.

Darke, I., Davidson-Arnott, R., Ollerhead, J., 2009. Measurement of beach surface moisture using surface brightness. J. Coastal Res. 251, 248–256.

Davidson-Arnott, R., 2010. Introduction to Coastal Processes and Geomorphology. Cambrigde University Press, The Edinburgh Building, Cambridge CB2 8RU, UK.

Davidson-Arnott, R., Law, M., 1996. Measurement and prediction of long-term sediment supply to coastal foredunes. J. Coastal Res. 12 (3), 654–663.

Davidson-Arnott, R.G.D., MacQuarrie, K., Aagaard, T., 2005. The effect of wind gusts, moisture content and fetch length on sand transport on a beach. Geomorphology 68, 115–129.

De Winter, R., Gongriep, F., Ruessink, B., 2015. Observations and modeling of alongshore variability in dune erosion at Egmond aan Zee, the Netherlands. Coast. Eng. 99, 167–175.

Delgado-Fernandez, I., 2010. A review of the application of the fetch effect to modelling sand supply to coastal foredunes. Aeolian Res. 2 (2–3), 61–70.

Delgado-Fernandez, I., 2011. Meso-scale modelling of aeolian sediment input to coastal dunes. Geomorphology 130 (3–4), 230–243.

Delgado-Fernandez, I., Davidson-Arnott, 2009. Sediment input to foredunes: description and frequency of transport events at Greenwich Dunes, PEI, Canada. J. Coastal Res. 56, 302–306.

Edwards, B.L., Namikas, S.L., DSa, E.J., 2013. Simple infrared techniques for measuring beach surface moisture. Earth Surf. Proc. Land. 38, 192–197.

Fecan, F., Marticorena, B., Bergametti, G., 1999. Parametrization of the increase of the aeolian erosion threshold wind friction velocity due to soil moisture for arid and semi-arid areas. Ann. Geophysicae-Atmos. Hydrospheres Space Sci. 17, 149–157.

Heritage, G., 2009. Laser Scanning for the Environmental Sciences. Wiley-Blackwell. iSBN: 978-1-4051-5717-9.

Hesp, P.A., Walker, I.J., Namikas, S.L., Davidson-Arnott, R.B., Bauer, B.O., Ollerhead, 2009. Storm wind flow over a foredune, prince edward island, Canada. J. Coastal Res. 1, 312–316.

Hillel, D., 1980. Fundamental of Soil Physics. Academic, New York.

Höfle, B., Pfeifer, N., 2007. Correction of laser scanning intensity data: data and model-driven approaches. J. Photogrammetry Remote Sens. 62, 415–433.

Jensen, J.R., 2007. Remote Sensing of the Environment: An Earth Resource Perspective. Pearson.

Kaasalainen, S., Niittymäki, H., Krooks, A., Koch, K., Kaartinen, H., Vain, A., Hyyppä, H., 2010. Effect of target moisture on laser scanner intensity. IEEE Trans. Geosci. Remote Sens. 48 (4), 2128–2136.

Kaasalainen, S., Jaakkola, A., Kaasalainen, M., Krooks, A., Kukko, A., 2011. Analysis of incidence angle and distance effects on terrestrial laser scanner intensity: search for correction methods. Remote Sens. 3, 2207–2221.

Keijsers, J., De Groot, A., Riksen, M., 2016. Modeling the biogeomorphic evolution of coastal dunes in response to climate change. J. Geophys. Res. Earth Surf. 121 (6), 1161–1181. http://dx.doi.org/10.1002/2015JF003815.

Kukko, A., Kaasalainen, S., Litkey, P., 2008. Effect of incidence angle on laser scanner intensity and surface data. Appl. Opt. 47 (7), 986–992.

Leu, D.J., 1977. Visible and near-infrared reflectance of beach sands: a study on the spectral reflectance/grain size relationship. Remote Sens. Environ. 6, 169–182.

Lobell, D., Asner, G., 2002. Moisture effects on soil reflectance. Soil Sci. Soc. Am. J. 66, 722–727.

Marticorena, B., Bergametti, G., 1995. Modeling the atmospheric dust cycle: 1. Design of a soil-derived dust emission scheme. J. Geophys. Res. Planets 100, 16415–16430.

McKenna Neuman, C., Scott, M.M., 1998. A wind tunnel study of the influence of pore water on aeolian sediment transport. J. Arid Environ. 39, 403–419.

McTainsh, G.H., Lynch, A.W., Tews, E.K., 1998. Climatic controls upon dust storm occurrence in eastern Australia. J. Arid Environ. 39, 457–466.

Namikas, S.L., Edwards, B.L., Bitton, M.C.A., Booth, J.L., Zhu, Y., 2010. Temporal and spatial variabilities in the surface moisture content of a fine-grained beach. Geomorphology 114, 303–310.

Nield, J.M., Wiggs, G.F.S., Squirrell, R.S., 2011. Aeolian sand strip mobility and protodune development on a drying beach: examining surface moisture and surface roughness patterns measured by terrestrial laser scanning. Earth Surf. Proc. Land. 36, 513–522.

Nield, J.M., King, J., Jacobs, B., 2014. Detecting surface moisture in aeolian environments using terrestrial laser scanning. Aeolian Res. 12, 9–17.

Nolet, C., Poortinga, A., Roosjen, P., Bartholomeus, H., Ruessink, G., 2014. Measuring and modeling the effect of surface moisture on the spectral reflectance of coastal beach sand. PLoS One.

Pesci, A., Teza, G., 2008. Effects of surface irregularities on intensity data from laser scanning: an experimental approach. Ann. Geophys. 51 (5), 839–848.

Roelvink, D., Reniers, A., van Dongeren, A., van Thiel de Vries, J., McCall, R., Lescinski, J., 2009. Modelling storm impacts on beaches, dunes and barrier islands. Coast. Eng. 56 (11), 1133–1152.

Sarre, R.D., 1988. Evaluation of aeolian sand transport equations using intertidal zone measurements, Saunton Sands, England. Sedimentology 35, 671.

Schmutz, P.P., Namikas, S.L., 2011. Utility of the Delta-T theta probe for obtaining surface moisture measurements from beaches. J. Coastal Res. 27 (3), 478–484.

Shuchman, R.A., Rea, D.K., 1981. Determination of beach sand parameters using remotely sensed aircraft reflectance data. Remote Sens. Environ. 11, 295–310.

Tsegaye, T.D., Tadesse, W., Coleman, T.L., Jackson, T.J., Tewolde, H., 2004. Calibration and modification of impedance probe for near surface soil moisture measurements. Can. J. Soil Sci. 84, 237–243.

Van Enckevort, I.M.J., Ruessink, B.G., 2001. Effect of hydrodynamics and bathymetry on video estimates of nearshore sandbar position. J. Geophys. Res. 106. http://dx.doi.org/10.1029/1999JC000167.

Wagner, W., Ullrich, A., Ducic, V., Melzer, T., Studnicka, N., 2006. Gaussian decomposition and calibration of a novel small-footprint full-waveform digitising airborne laser scanner. J. Photogrammetry Remote Sens. 60, 100–112.

Walker, I.J., Davidson-Arnott, R.G.D., Bauer, P.A.H.B.O., Ollerhead, J., 2009. Mean flow and turbulence responses in airflow over foredunes: new insights from recent research. J. Coastal Res. 1, 366–370.

Wallace, J.M., Hobbs, P.V., 2006. . Atmoshperic Science; An Introductory Survey, International Geophysics Series, second ed., vol. 92. Academic Press.

Watson, R.D., 1970. Surface-coating effects in remote sensing measurements. J. Geophys. Res. 75 (2), 480–484.

Wiggs, G.F.S., Baird, A.J., Atherton, R.J., 2004. The dynamic effects of moisture on the entrainment and transport of sand by wind. Geomorphology 59, 13–30.